

NASA TECHNICAL NOTE



NASA TN D-3388

NASA TN D-3388

LOAN COPY: RE
APPL (WLI
KIRTLAND AFB,

0130232



TECH LIBRARY KAFB, NM

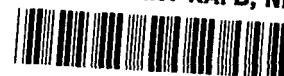
EFFECTS OF BLUNTNESS ON THE SUBSONIC DRAG OF AN ELLIPTICAL FOREBODY

by John D. Norris and Robert J. McGhee

Langley Research Center

Langley Station, Hampton, Va.

TECH LIBRARY KAFB, NM



0130232

NASA TN D-3388

EFFECTS OF BLUNTNESS ON THE SUBSONIC DRAG
OF AN ELLIPTICAL FOREBODY

By John D. Norris and Robert J. McGhee

Langley Research Center
Langley Station, Hampton, Va.

NATIONAL AERONAUTICS AND SPACE ADMINISTRATION

For sale by the Clearinghouse for Federal Scientific and Technical Information
Springfield, Virginia 22151 - Price \$0.30

EFFECTS OF BLUNTNESS ON THE SUBSONIC DRAG OF AN ELLIPTICAL FOREBODY

By John D. Norris and Robert J. McGhee
Langley Research Center

SUMMARY

An investigation has been conducted in the Langley 8-foot transonic pressure tunnel to determine the effects of forebody bluntness on the subsonic drag coefficient of a family of elliptical forebodies in combination with a cylindrical afterbody. Most of the tests were conducted at a constant Reynolds number of 6.3×10^6 (based on length of cylindrical afterbody) through a Mach number range from 0.20 to 0.90. In addition, at a Mach number of 0.60, tests were conducted over a Reynolds number range from approximately 4.1×10^6 to 13.3×10^6 . All tests were conducted at 0° angle of attack.

The results indicate that increasing the forebody bluntness rapidly decreased the drag-rise Mach number, except where flow separation ahead of the forebody shoulder occurred. The presence of shock systems at the high subsonic Mach numbers steepens the pressure gradient and promotes separation for moderate forebody bluntness. It appears that for a Mach number equal to or less than 0.60 a bluntness ratio as low as 0.65 can be tolerated before a large increase in drag occurs.

INTRODUCTION

With the advent of some of the newer space vehicle systems there has been an increased interest in the aerodynamic characteristics of basic blunt forebody-cylinder combinations which would be representative of stages of reusable launch vehicles or tankage systems. For conceptual reusable launch vehicles the first stage would separate, after its initial lift-off boost, and fly back and make a horizontal landing. A blunt forebody shape would result in a significant reduction in interstage weight and hence large payloads but may also result in a higher drag during first-stage flyback to the recovery site. Consequently it is important to have meaningful aerodynamic inputs so that the trade off between aerodynamic characteristics and interstage weight can be optimized. The available information relating the effects of forebody bluntness on drag was for various afterbody shapes and different Reynolds numbers. Most of the reported data, such as references 1 and 2, are for Reynolds numbers for which laminar flow would be expected over the forebody.

The present investigation was initiated to determine the drag characteristics of a family of elliptical forebodies in combination with cylindrical afterbodies and varying from a hemisphere to a plane nose; the tests were made at large Reynolds numbers for which turbulent flow exists over the forebodies.

The investigation was conducted in the Langley 8-foot transonic pressure tunnel at subsonic Mach numbers from 0.20 to 0.90. Most of the tests were conducted at a constant Reynolds number of 6.3×10^6 (based on length of cylindrical afterbody) for the Mach number range; at a Mach number of 0.60 additional tests were conducted over a Reynolds number range from approximately 4.1×10^6 to 13.3×10^6 .

SYMBOLS

The units used for the physical quantities defined in this paper are given both in U.S. Customary Units and in the International System of Units (SI).

A	cross-sectional area of cylindrical afterbody, $\frac{\pi d^2}{4}$, 0.4295 foot ² (399 centimeter ²)
a	semiminor axis of elliptical forebody (fig. 1)
b	semimajor axis of elliptical forebody (fig. 1)
C_D	drag coefficient, $C_{D,t} - C_{D,b}$
$C_{D,b}$	base drag coefficient, $\frac{\text{Base drag}}{qA}$
$C_{D,f}$	forebody drag coefficient, $C_D - C_F \frac{S_w}{A}$
$C_{D,t}$	total drag coefficient, $\frac{\text{Total drag}}{qA}$
C_F	average turbulent skin-friction coefficient of cylindrical afterbody
d	diameter of cylindrical afterbody, 8.875 inches (22.543 centimeters)
M	free-stream Mach number
q	free-stream dynamic pressure, pounds per foot ² (newtons per meter ²)
R	Reynolds number based on cylindrical afterbody length of 31.500 inches (80.010 centimeters)

S_w	wetted area of cylindrical afterbody, 6.960 foot ² (6466 centimeter ²)
x,y	rectangular coordinates (fig. 1)

APPARATUS AND TESTS

Models

The model consisted of a cylindrical body with various forebodies attached. Details of a family of elliptical forebodies are shown in figure 1 and photographs of the basic model and the forebodies are presented in figure 2. The basic cylindrical afterbody had a length-diameter ratio of 3.55. Each forebody was constructed so that the nose-cylinder juncture did not coincide with the end of the forebody, but was 1 inch (2.54 cm) rearward of the forebody shape on the cylindrical afterbody. The forebody coordinates were determined from the expression for an ellipse $\frac{x^2}{a^2} + \frac{y^2}{b^2} = 1$. (See fig. 1.) Six forebodies were tested in combination with the cylindrical afterbody; the nose or forebody shape varied from a hemisphere ($\frac{a}{b} = 1$) to the limiting case of a flat or plane nose ($\frac{a}{b} = 0$). The six forebody shapes, identified as configurations 1 to 6, are shown in figures 1 and 2.

Tests

The investigation was conducted in the Langley 8-foot transonic pressure tunnel. The six configurations were tested at Mach numbers of 0.20, 0.40, 0.60, and 0.80 (configuration 1 was also tested at Mach numbers of 0.30, 0.50, 0.70, and 0.90) for a constant Reynolds number of 6.3×10^6 , based on the length of the cylindrical afterbody. (See fig. 3.) The six configurations were also tested over a Reynolds number range from approximately 4.1×10^6 to 13.3×10^6 at a Mach number of 0.60. All tests were conducted at 0° angle of attack.

The drag acting on the models was measured by an internal strain-gage balance located in the cylindrical afterbody. Static pressures at the base of the model were measured and the total drag coefficient $C_{D,t}$ has been adjusted to correspond to the conditions of free-stream static pressure acting at the model base; hence, the drag coefficient shown as C_D is the sum of the forebody pressure and skin friction and the afterbody skin friction. The estimated accuracy of $C_{D,t}$ based on instrument calibration for $R = 6.3 \times 10^6$ is ± 0.003 at $M = 0.80$ and ± 0.043 at $M = 0.20$.

Methods

Many of the previous tests were conducted at Reynolds numbers and surface conditions for which most of the flow over the forebody would probably be laminar. (See refs. 1 and 2.) In an attempt to insure that turbulent flow existed over the forebodies for

the present investigation, a 0.10-inch-wide strip of No. 80 carborundum grains was applied to the forebody section at a location determined by a 40° angle measured from the forebody center line at $x = 0$ for configurations 1 to 4 and at 50 percent of the forebody radius for configurations 5 and 6. References 3 and 4 were used as a guide to determine the grit size necessary to insure boundary-layer transition.

Oil-flow pictures were taken during phases of the wind-tunnel investigation in order to ascertain the types of flow and flow patterns over the forward section of the models. This technique (described in detail in ref. 5) consists of spreading a fluorescent-oil film over the model and viewing the flow pattern and relative densities under ultraviolet light.

The average turbulent skin-friction coefficient of the cylindrical afterbody C_F was computed by using the Kármán-Schoenherr equation for incompressible flow and the Sommer and Short T' method to correct for compressibility effects (Appendix B of ref. 6). The forebody drag coefficient presented herein $C_{D,f}$ therefore is the external drag coefficient C_D decreased by the calculated skin-friction drag coefficient. For the entire investigation turbulent flow was considered to exist on the cylindrical afterbody and no account has been taken of the effect of any regions of flow separation on the afterbody skin-friction drag coefficient.

RESULTS AND DISCUSSION

The results of this investigation have been divided into two parts; the first consists of oil-flow pictures of selected configurations and the second consists of the basic data for the six configurations. Figures 4 and 5 illustrate the flow patterns over the forebody portion of the models. Figure 6 presents the drag coefficient C_D and the base drag coefficient $C_{D,b}$ plotted against Mach number for configuration 1 with and without carborundum transition strips. In figures 7, 8, and 9 the drag coefficient C_D is presented as a function of Mach number, bluntness ratio or forebody shape, and Reynolds number, respectively, for the different configurations tested. In order to determine the effects of forebody shape only, the turbulent skin-friction drag coefficient of the cylindrical afterbody was calculated and subtracted from the drag coefficient C_D to give the net forebody drag coefficient $C_{D,f}$. The forebody drag coefficients for the various configurations were normalized to $C_{D,f}$ for configuration 1 (the hemispherical forebody) and this normalized coefficient $\frac{C_{D,f}}{(C_{D,f})_1}$ is presented in figures 10 and 11 as a function of Mach number and of forebody shape, respectively.

Flow Characteristics

In order to establish what type of flow existed over the forebody section, oil-flow photographs were obtained over a range of Reynolds numbers at $M = 0.60$ for configuration 1 and over a range of Mach numbers for all configurations at a constant Reynolds number of 6.3×10^6 . Configuration 1 was tested with various surface conditions, and oil-flow pictures were taken of the resulting flow patterns. Figure 4 shows a comparison of the oil-flow pictures for a constant Reynolds number of 6.3×10^6 at $M = 0.60$ and 0.80 for configuration 1 with the forebody surface smooth and with the transition strip located as described previously. Thus, from the photographs for $M = 0.60$ (figs. 4(a) and 4(b)), it can be seen that laminar flow exists over the smooth forebody surface with separation occurring at the shoulder, whereas an early transition occurs and turbulent flow exists over the forebody with transition strips and there is little evidence of separation occurring at the shoulder. The high shearing action of turbulent flow is characterized by the streaks in the oil film whereas laminar flow with its lower surface shear stress leaves a thicker oil film and, consequently, a brighter picture. The oil tends to pile up in the separated regions as shown in figures 4(a) and 4(c). Figures 4(c) and 4(d) indicate that at $M = 0.80$ local critical speeds may have been reached near the forebody shoulder and have resulted in shock-induced separation.

Figure 5 shows the effect of Mach number for configuration 2 ($a/b = 0.67$) with a transition strip on the forebody and indicates that turbulent flow existed over the forebody region for a Reynolds number of 6.3×10^6 for the entire test Mach number range. Figure 5(c) shows evidence of a shock system at $M = 0.60$ by the bright concentration of oil approximately at the shoulder. Figure 5(d) shows the shock system present which resulted in separation near the shoulder at $M = 0.80$. From evaluation of all the oil-flow data, of which figures 4 and 5 are representative, it is concluded that with a transition strip consisting of No. 80 carborundum grains located on the forebody turbulent flow was obtained for configurations 1 to 5 at all Mach numbers for which the test Reynolds number exceeded about 6.0×10^6 .

External Drag Coefficient

The drag coefficient C_D and the base drag coefficient $C_{D,b}$ are plotted in figure 6 against Mach number for configuration 1. The forebody was tested with the surface smooth, with a carborundum transition strip applied at the forebody shoulder, and with a carborundum transition strip on the forebody. It is evident that the transition strip applied at the shoulder had little or no effect on C_D ; however, above $M = 0.60$, the transition strip added to the forebody caused a reduction in C_D . As previously discussed, figures 4(c) and 4(d) showed that, at $M = 0.80$, flow separation occurred earlier on the forebody with laminar flow than with turbulent flow. This occurrence therefore

explains the reduction in C_D which would result from the larger negative pressures achievable in the shoulder region for turbulent flow.

Figure 7 presents the variation of C_D and $C_{D,b}$ with Mach number at a constant Reynolds number of 6.3×10^6 for configurations 1 to 6. It can be seen that blunting the forebody causes the drag rise to occur at a lower Mach number. The drag rise for configurations 1, 2, and 3 is probably a result of the presence of a shock system which steepens the pressure gradient and promotes separation. The initial high level of drag for configurations 4, 5, and 6 is believed to have resulted from early flow-induced separation ahead of the shoulder. For flow already separated ahead of the shoulder, the effect of Mach number induced separation is of secondary importance. A correlation of various experimental drag data was made in reference 1 for cylinders with hemispherical and plane noses. The results of the present investigation generally indicate lower levels of drag coefficient than those of reference 1 – probably a result of the existence of some flow-induced separation at the shoulder for the data of reference 1. The forebody drag coefficient $C_{D,f}$ for configuration 1 is also shown in figure 7 for comparison.

Blunting the forebody caused a reduction in the base drag coefficient $C_{D,b}$ as shown in figure 7. For configuration 6 the most significant change in $C_{D,b}$ occurred at $M = 0.80$ where $C_{D,b}$ is almost zero, a value indicating that the pressure at the base of the model was approximately equal to the free-stream pressure. The results presented in reference 7 indicate that for a flat-faced forebody shape the flow separates tangentially at the shoulder and reattaches downstream on the afterbody with a resulting increase in pressure due to the reattachment and mixing associated with the turbulent eddies of the separated vortex. From reference 7, the reattachment for the present model would be expected to occur near the base of the cylindrical afterbody and to result in the higher base pressures shown. It is concluded, therefore, that at least for the two bluntest forebodies, configurations 5 and 6, significant regions of flow separation over the afterbody were probably present.

Figure 8 presents the drag coefficient C_D plotted against the bluntness ratio a/b for the test Mach number range. It can be seen that some blunting ($a/b < 1$) can be tolerated below $M = 0.60$ before the onset of serious increases in drag coefficient associated with flow separation. For example, the data indicate that values of a/b from 1 to about 0.65 provide approximately the same values of drag coefficient for $M \leq 0.60$.

All six configurations were tested through a Reynolds number range from about 4.1×10^6 to 13.3×10^6 at $M = 0.60$ and the results are shown in figure 9. Turbulent flow was probably achieved on the forebody for configurations 1 and 2 with no separation and low drag coefficients resulted. Configurations 3 to 6 show the highest values of C_D , probably resulting from the laminar flow separation discussed earlier for the forebodies at the lower Reynolds numbers. As the Reynolds number was increased the flow over the

forebody became turbulent and the separation point moved rearward, thereby decreasing C_D for configurations 3 to 5. For configuration 6 it would be expected that Reynolds number would not affect the drag level since separation would occur at the shoulder for this flat-faced configuration regardless of laminar or turbulent flow existing on the forebody. The forebody drag coefficient $C_{D,f}$ for configuration 1 has been included in the figure for reference. Figure 9 also shows the drag coefficient from unpublished data from another test (in the Langley 8-foot transonic pressure tunnel) for a cylindrical body with a length-diameter ratio of 4 and an elliptical forebody shape corresponding to $a/b = 1$ with a transition strip located at the juncture of the forebody and cylinder. It is seen that, even at a Reynolds number of 3.2×10^6 , the drag level is in good agreement with the results of the present test.

Forebody Drag Coefficient

Figure 10 presents the forebody drag coefficient normalized to the forebody drag coefficient of configuration 1 (hemispherical forebody) as a function of Mach number for configurations 2 to 6. Any flow separation on the cylindrical afterbody has not been taken into account on the afterbody skin-friction drag coefficient used in determining the normalized forebody drag coefficient. It can be seen that blunting the forebody increased $\frac{C_{D,f}}{(C_{D,f})_1}$ and that the increase in $\frac{C_{D,f}}{(C_{D,f})_1}$ varied from only a few percent, for configuration 2 over the Mach number range and for configuration 3 at the low Mach numbers, to values approaching 2 orders of magnitude above the drag coefficient for the basic hemispherical forebody. The large range of forebody drag at the low Mach numbers is associated with the flow-induced separation which did not occur for the reference forebody ($a/b = 1$), and the tendency for all values to converge at the highest test Mach number results from the fact that even the reference configuration has experienced a large transonic drag rise. The observed trend for an initial increase in the normalized drag coefficient prior to the transonic decrease shown for configurations 3, 4, and 5 is the result of the earlier drag rise associated with shock-induced separation over the shoulder. It is not clear, however, that any shock-induced separation existed for the flat-faced forebody, configuration 6. The data have also been plotted in figure 11 as a function of bluntness ratio a/b . As discussed previously, it is readily seen that, at $M \leq 0.60$, a bluntness ratio as low as about 0.65 can be tolerated before a large increase in forebody drag occurs.

CONCLUDING REMARKS

An investigation has been conducted in the Langley 8-foot transonic pressure tunnel to ascertain drag characteristics of a family of elliptical forebodies in combination with a

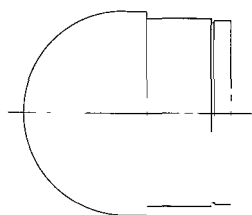
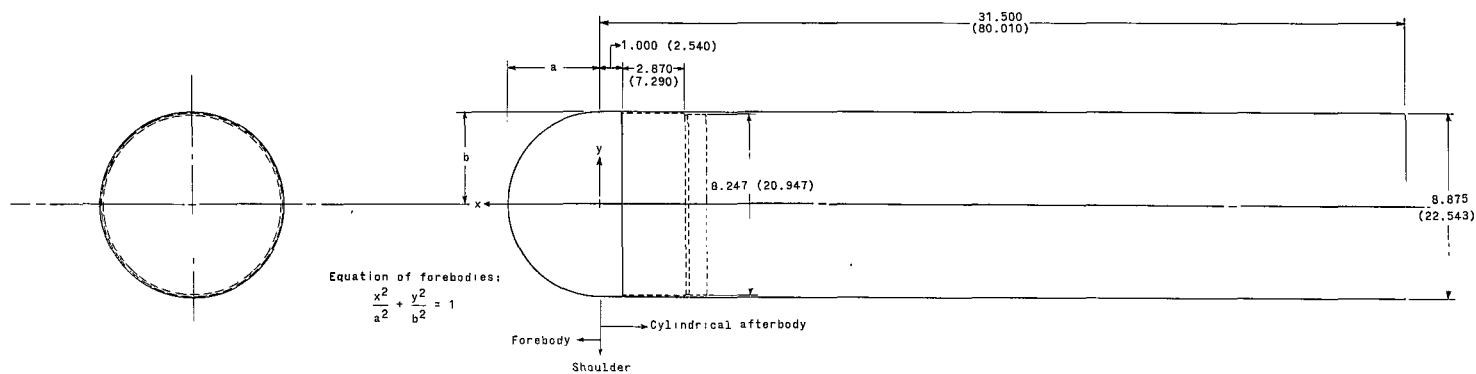
cylindrical afterbody and varying from a hemisphere to a flat or plane nose, with turbulent flow existing over the forebodies. Test data were obtained at a constant Reynolds number (based on length of cylindrical afterbody) of 6.3×10^6 for a subsonic Mach number range from 0.20 to 0.90 and through a Reynolds number range from approximately 4.1×10^6 to 13.3×10^6 at a Mach number of 0.60. All data were taken at 0° angle of attack.

The results indicate that increasing the forebody bluntness rapidly decreases the drag-rise Mach number, except where flow separation ahead of the shoulder occurs. The presence of shock systems at the high subsonic Mach numbers steepens the pressure gradient and promotes separation for moderate forebody bluntness. It appears that for a Mach number equal to or less than 0.60 a bluntness ratio as low as about 0.65 can be tolerated before a large increase in drag occurs.

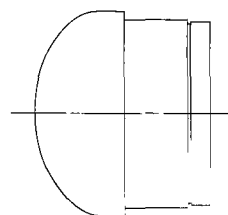
Langley Research Center,
National Aeronautics and Space Administration,
Langley Station, Hampton, Va., January 7, 1966.

REFERENCES

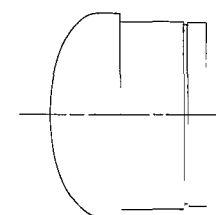
1. Stanbrook, A.: A Correlation of the Forebody Drag of Cylinders With Plane and Hemispherical Noses at Mach Numbers From Zero to 2.5. C.P. No. 709, Brit. A.R.C., 1964.
2. Polhamus, Edward C.: Effect of Nose Shape on Subsonic Aerodynamic Characteristics of a Body of Revolution Having a Fineness Ratio of 10.94. NACA RM L57F25, 1957.
3. Braslow, Albert L.; and Knox, Eugene C.: Simplified Method for Determination of Critical Height of Distributed Roughness Particles for Boundary-Layer Transition at Mach Numbers From 0 to 5. NACA TN 4363, 1958.
4. Tetervin, Neal: Theoretical Distribution of Laminar-Boundary-Layer Thickness, Boundary-Layer Reynolds Number and Stability Limit, and Roughness Reynolds Number for a Sphere and Disk in Incompressible Flow. NACA TN 4350, 1958.
5. Loving, Donald L.; and Katzoff, S.: The Fluorescent-Oil Film Method and Other Techniques for Boundary-Layer Flow Visualization. NASA MEMO 3-17-59L, 1959.
6. Peterson, John B., Jr.: A Comparison of Experimental and Theoretical Results for the Compressible Turbulent-Boundary-Layer Skin Friction With Zero Pressure Gradient. NASA TN D-1795, 1963.
7. Stanbrook, A.: Experimental Pressure Distributions on a Plane-Nosed Cylinder at Subsonic and Transonic Speeds. Tech. Note No. Aero. 2976, Brit. R.A.E., Mar. 1963.



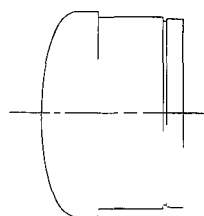
Configuration 1
 $a=4.437$ (11.270)
 $a/b=1$



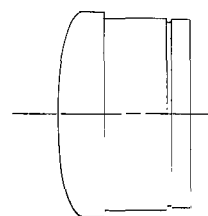
Configuration 2
 $a=2.959$ (7.516)
 $a/b=0.667$



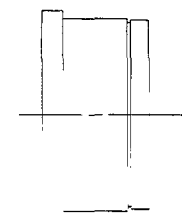
Configuration 3
 $a=2.219$ (5.636)
 $a/b=0.500$



Configuration 4
 $a=1.479$ (3.757)
 $a/b=0.333$

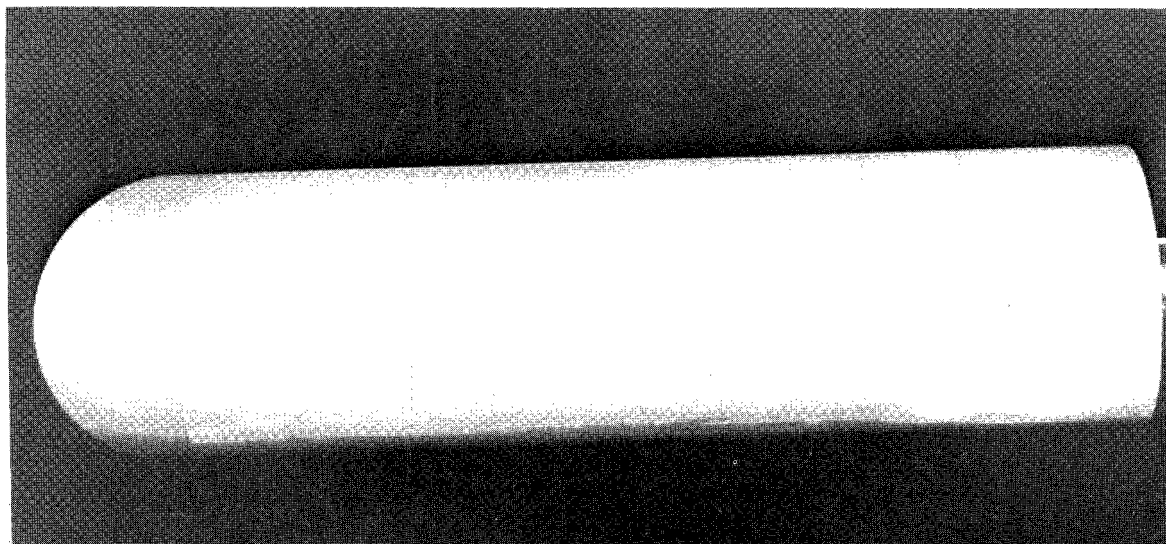


Configuration 5
 $a=1.109$ (2.817)
 $a/b=0.250$



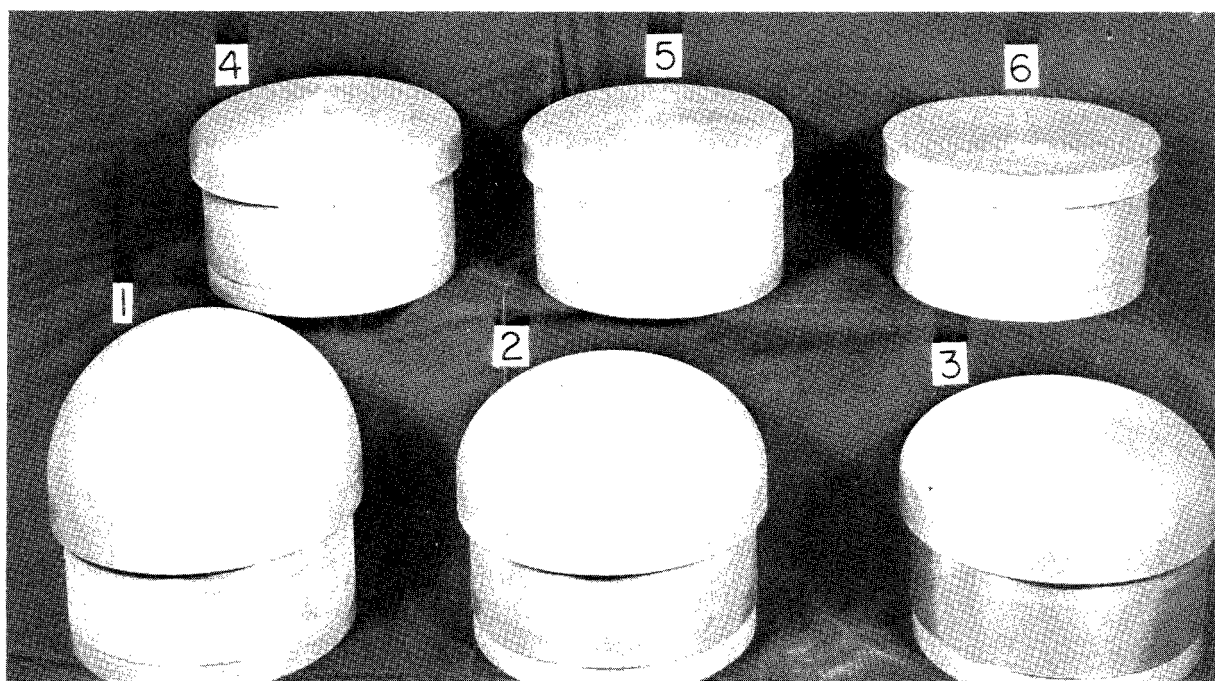
Configuration 6
 $a=0$
 $a/b=0$

Figure 1.- Details of elliptical forebodies and cylindrical afterbody. All dimensions are in inches (centimeters).



(a) Basic model.

L-64-5518



(b) Forebody configurations 1 to 6.

L-64-5520.1

Figure 2.- Photographs of configurations tested.

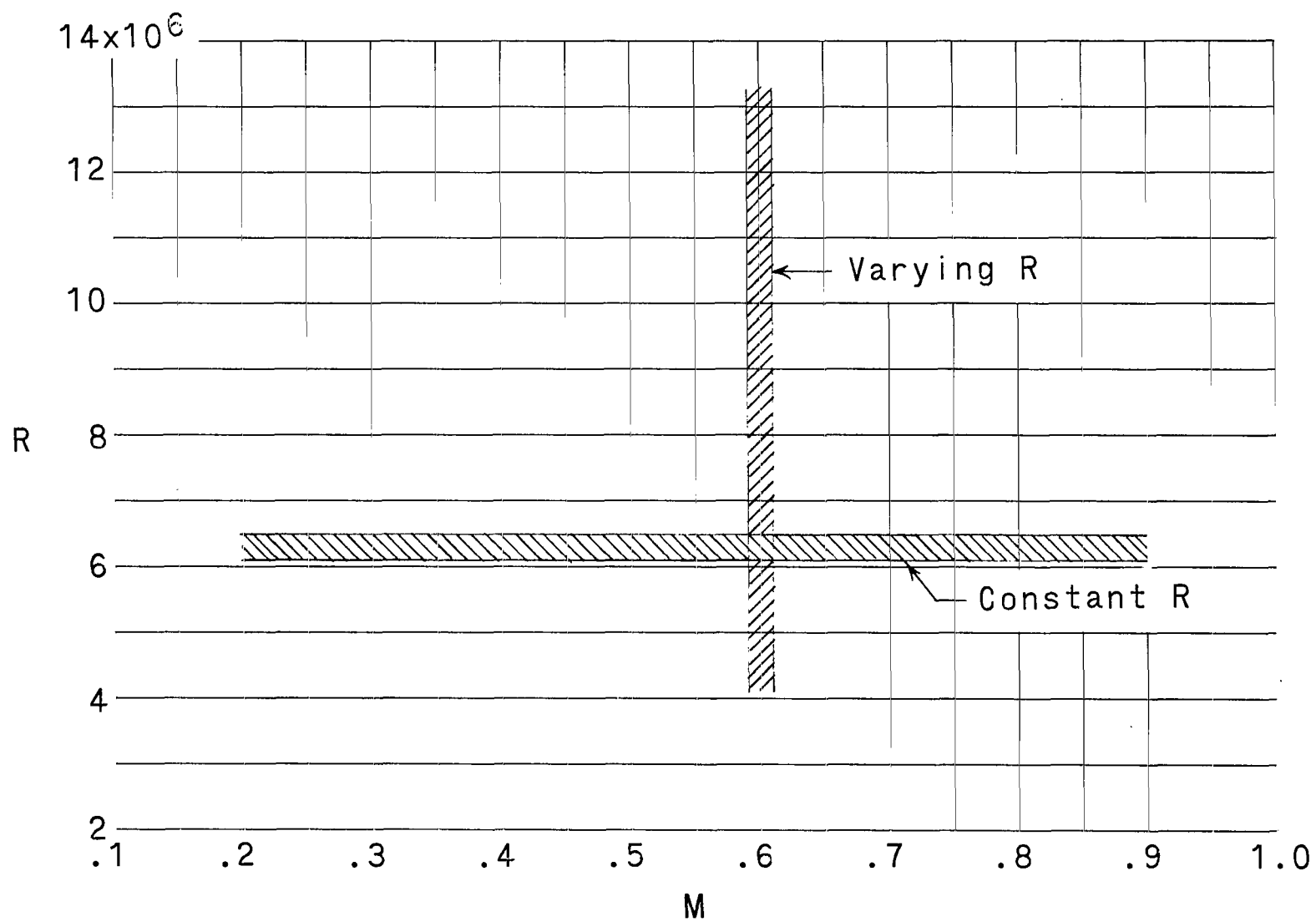
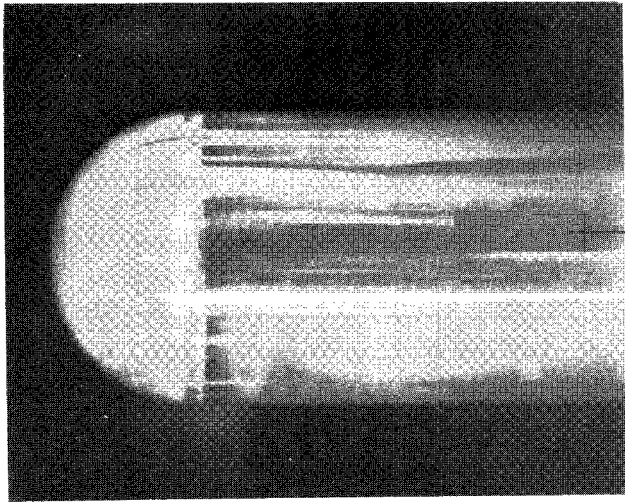
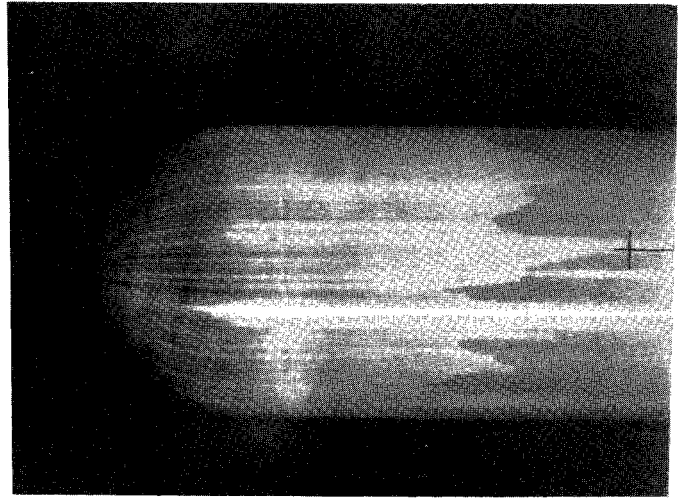


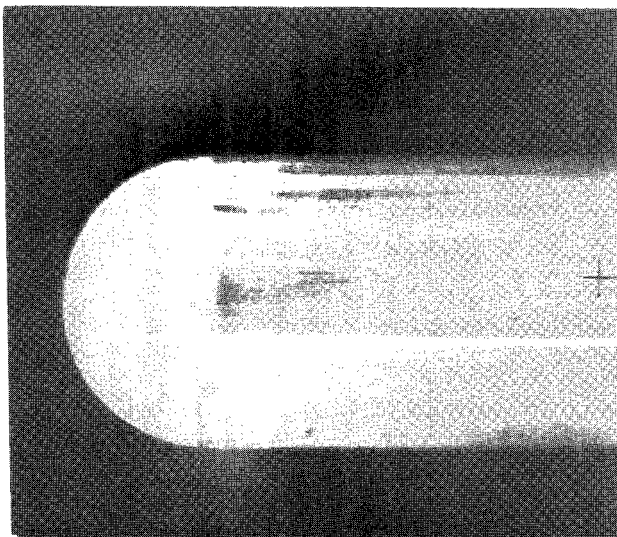
Figure 3.- Variation of Reynolds number with Mach number.



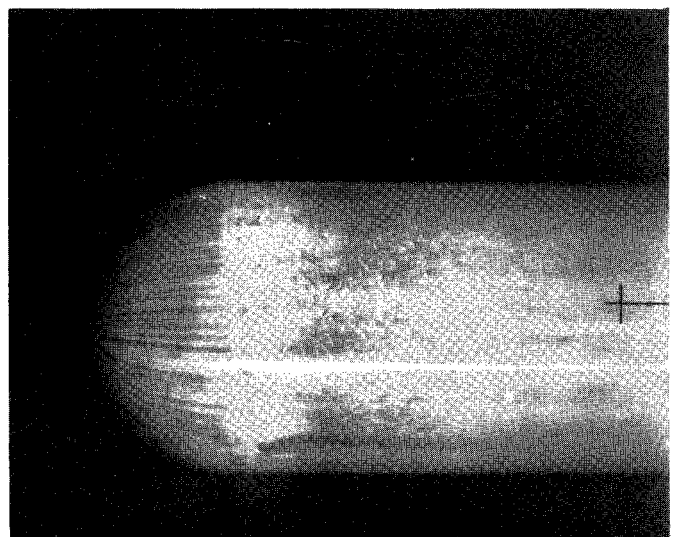
(a) Smooth; $M = 0.60$.



(b) Carborundum on forebody; $M = 0.60$.



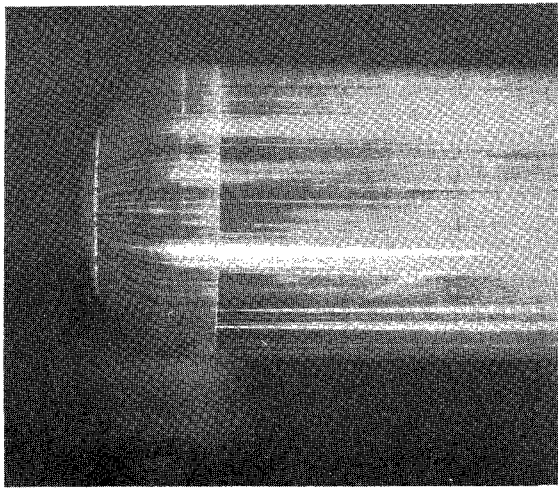
(c) Smooth; $M = 0.80$.



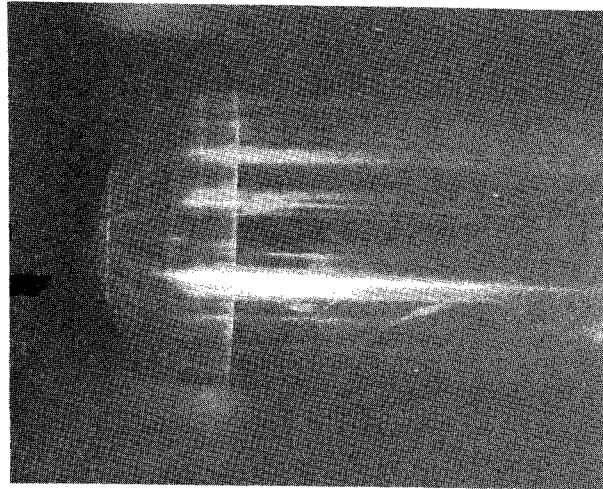
(d) Carborundum on forebody; $M = 0.80$.

L-66-1001

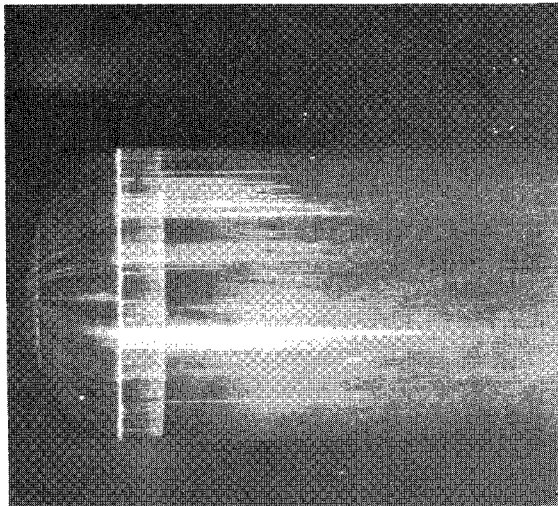
Figure 4.- Oil-flow photographs of configuration 1 ($\frac{a}{b} = 1.0$). $R = 6.3 \times 10^6$.



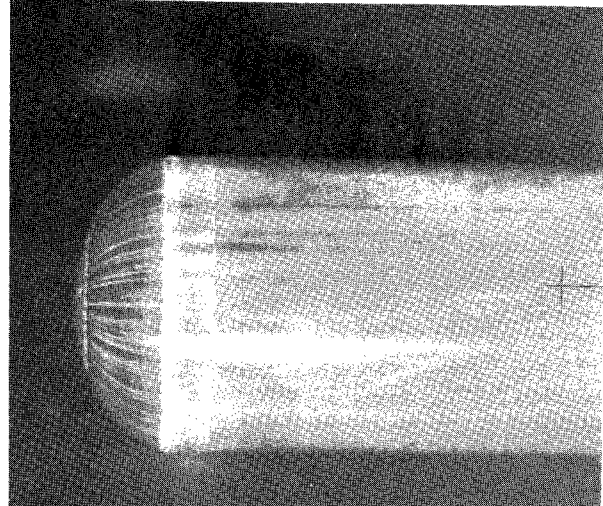
(a) $M = 0.20$.



(b) $M = 0.40$.



(c) $M = 0.60$



(d) $M = 0.80$.

L-66-1002

Figure 5.- Oil-flow photographs of configuration $2 \left(\frac{a}{b} = 0.67 \right)$ with transition strips. $R = 6.3 \times 10^6$.

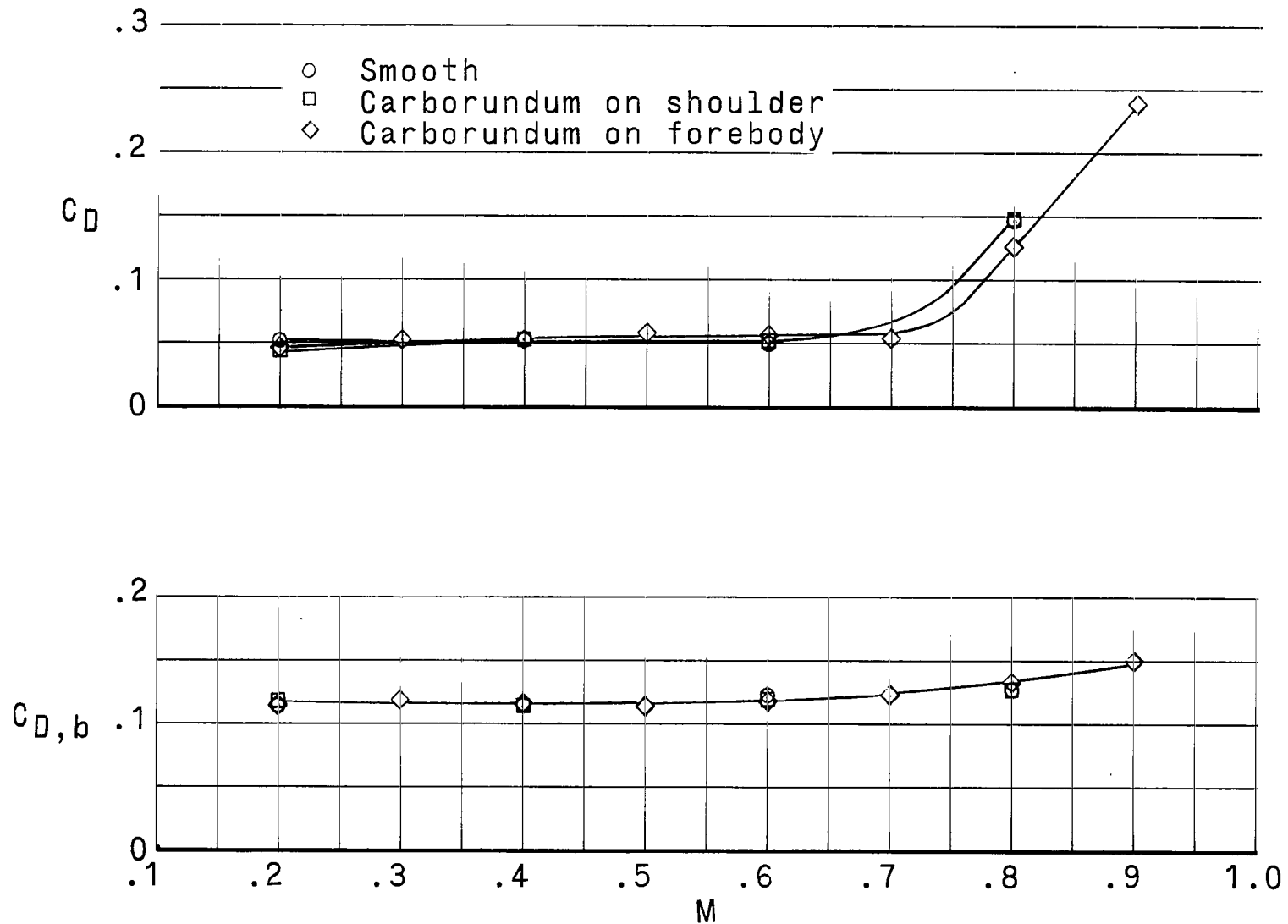


Figure 6.- Variation of C_D and $C_{D,b}$ with Mach number for configuration 1 ($\frac{a}{b} = 1.0$) with and without carborundum transition strip. $R = 6.3 \times 10^6$.

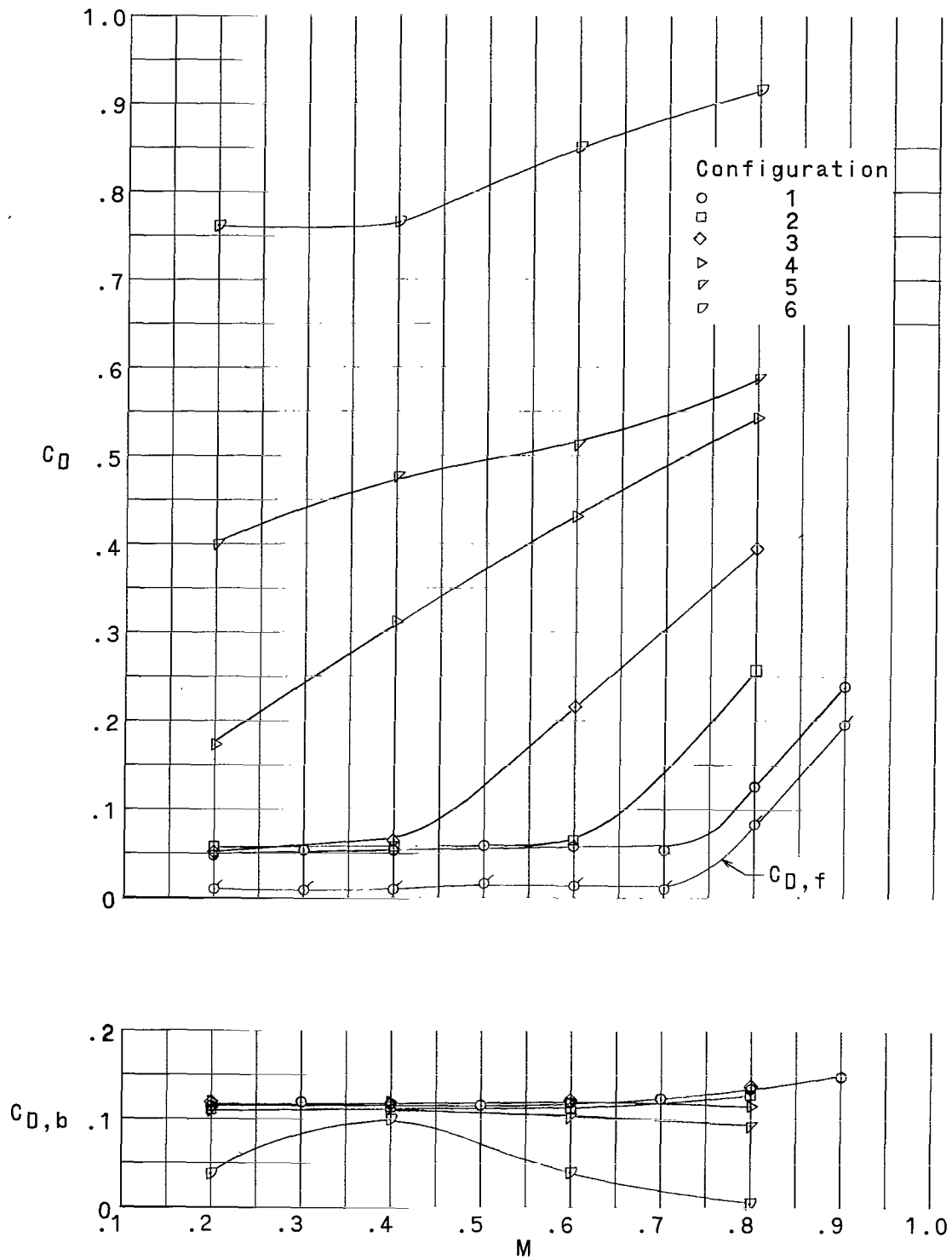


Figure 7.- Variation of C_D and $C_{D,b}$ with Mach number for configurations 1 to 6. $R = 6.3 \times 10^6$.

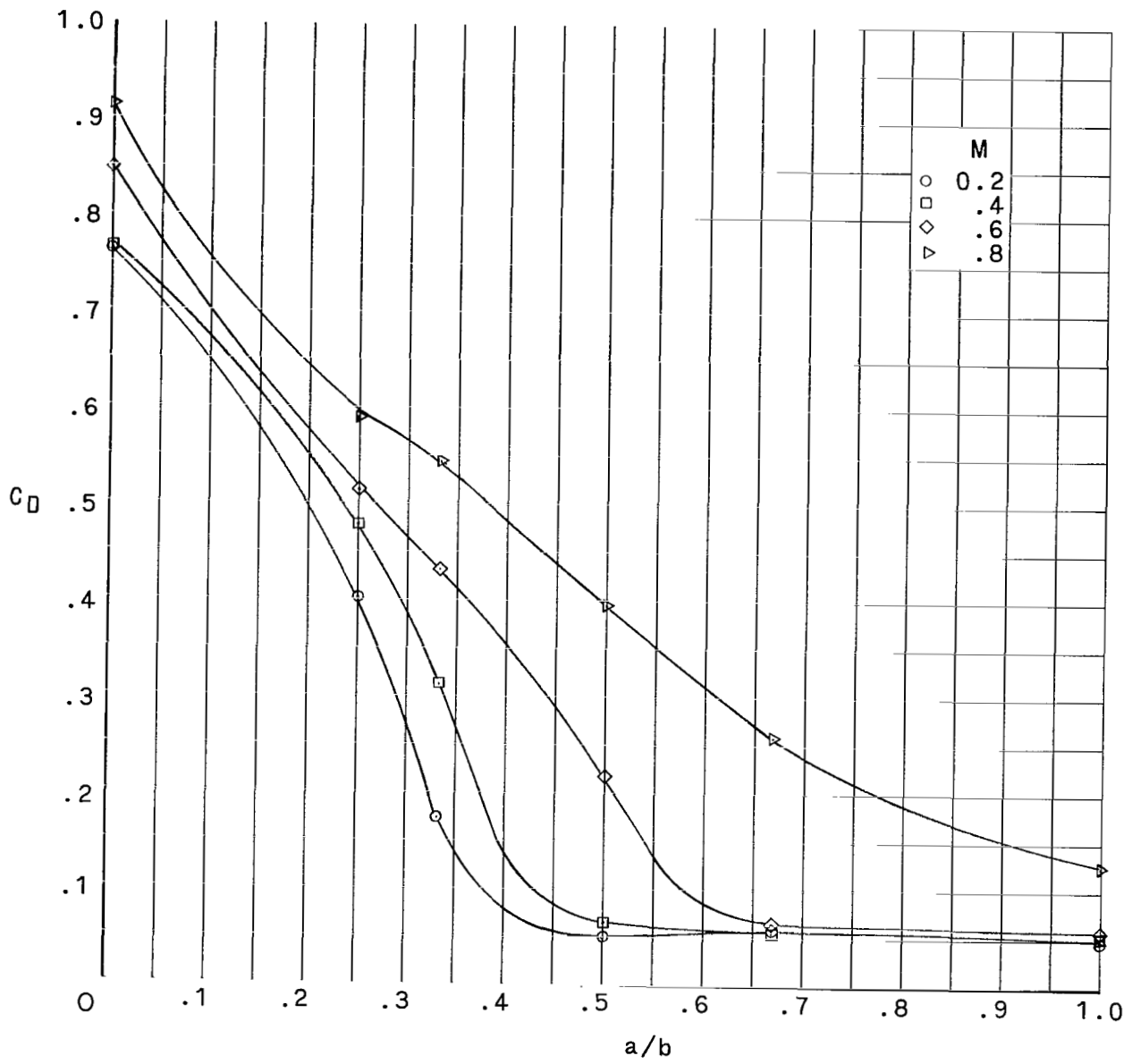


Figure 8.- Variation of C_D with bluntness ratio a/b . $R = 6.3 \times 10^6$.

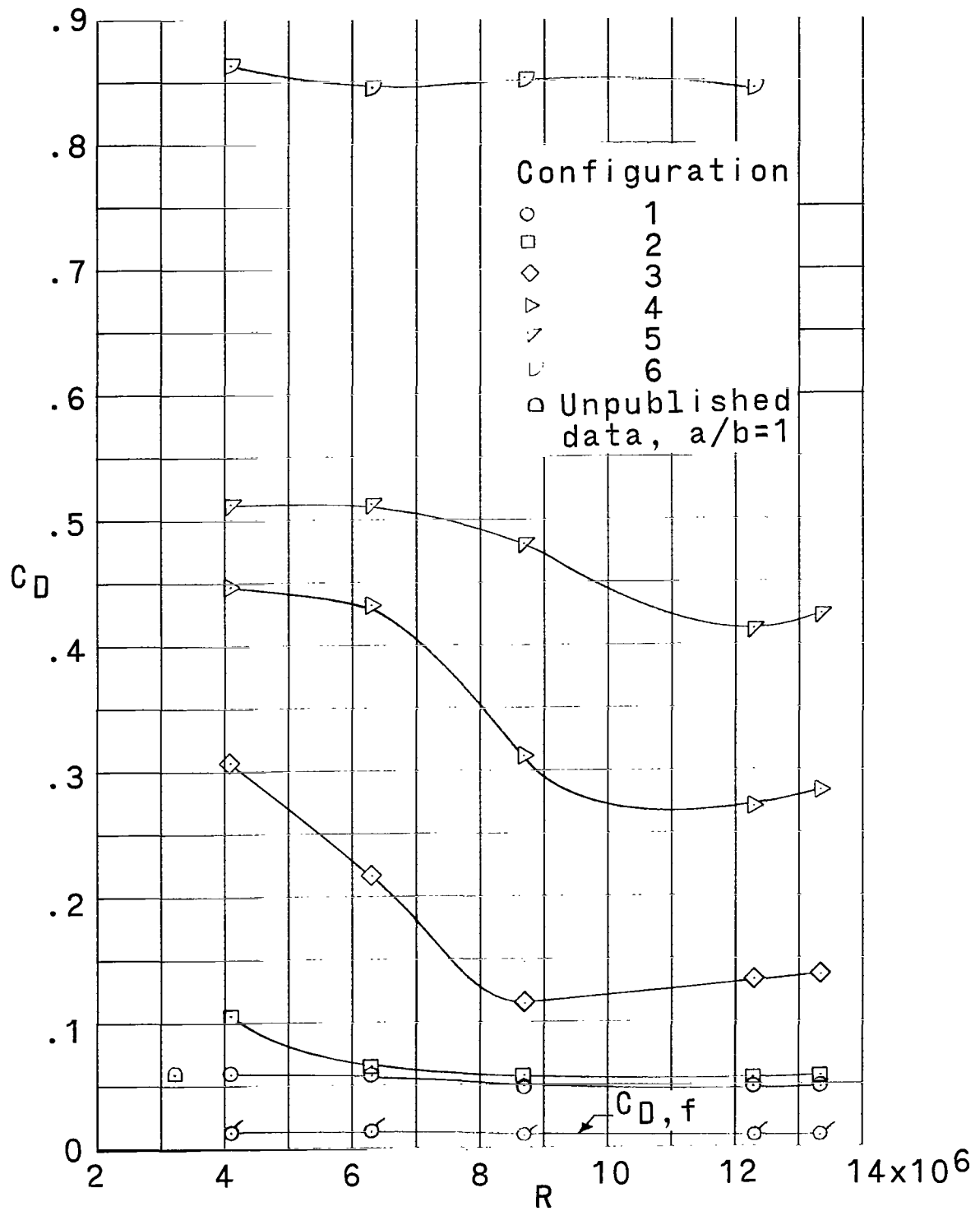


Figure 9.- Variation of C_D with Reynolds number. $M = 0.60$.

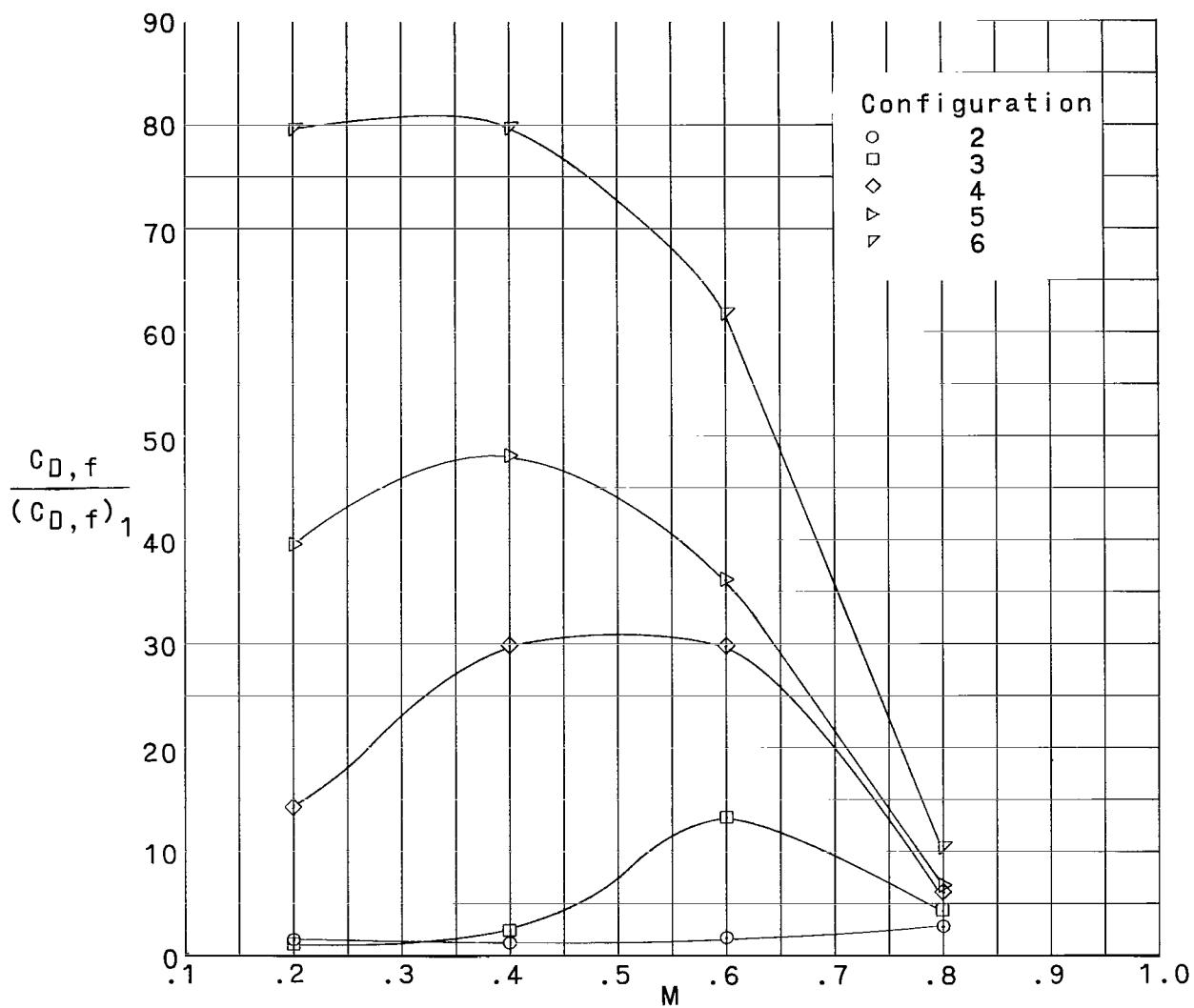


Figure 10.- Variation of normalized forebody drag coefficient $\frac{C_{D,f}}{(C_{D,f})_1}$ with Mach number. $R = 6.3 \times 10^6$.

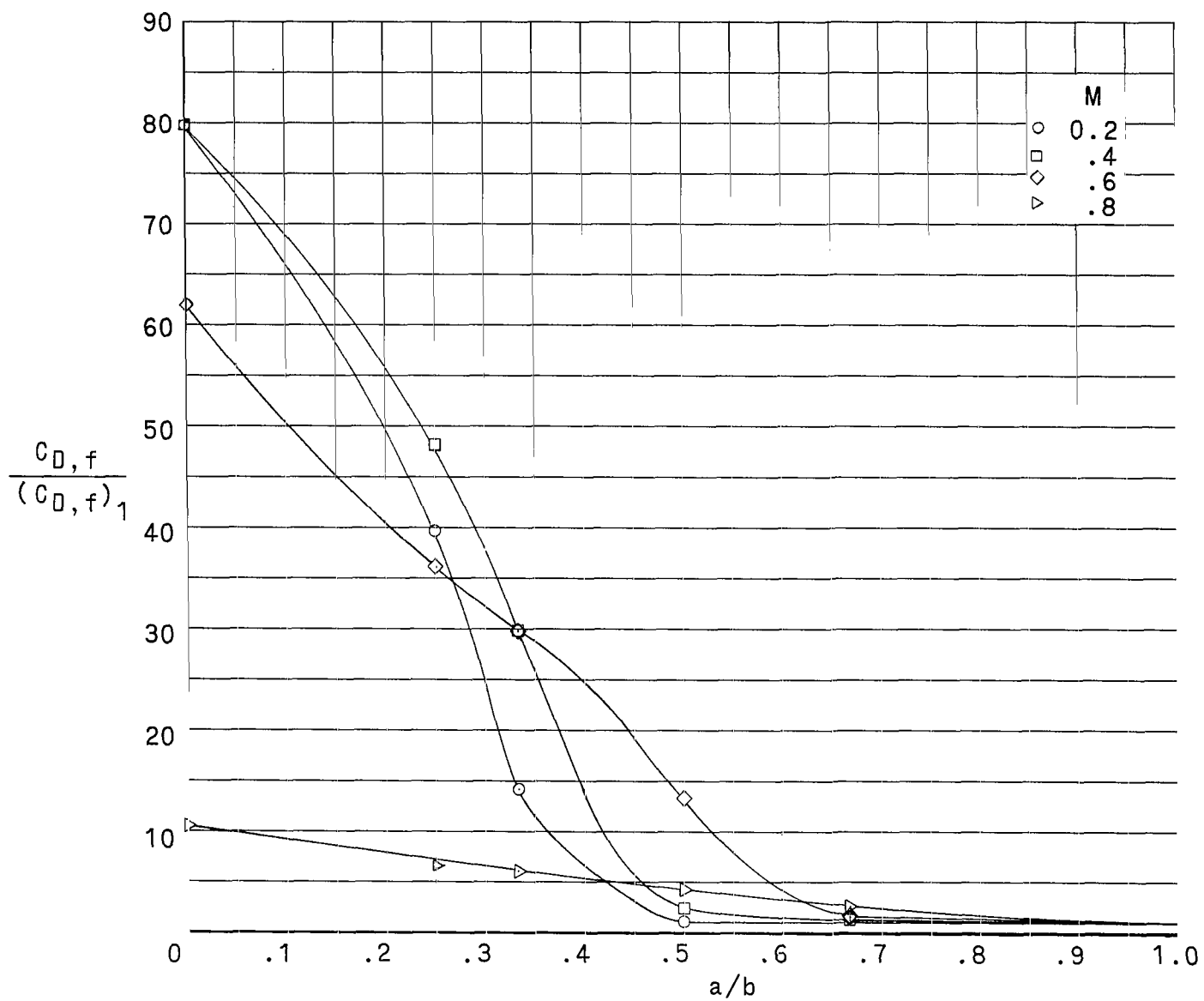


Figure 11.- Variation of normalized forebody drag coefficient $\frac{C_{D,f}}{(C_{D,f})_1}$ with bluntness ratio a/b . $R = 6.3 \times 10^6$.

"The aeronautical and space activities of the United States shall be conducted so as to contribute . . . to the expansion of human knowledge of phenomena in the atmosphere and space. The Administration shall provide for the widest practicable and appropriate dissemination of information concerning its activities and the results thereof."

—NATIONAL AERONAUTICS AND SPACE ACT OF 1958

NASA SCIENTIFIC AND TECHNICAL PUBLICATIONS

TECHNICAL REPORTS: Scientific and technical information considered important, complete, and a lasting contribution to existing knowledge.

TECHNICAL NOTES: Information less broad in scope but nevertheless of importance as a contribution to existing knowledge.

TECHNICAL MEMORANDUMS: Information receiving limited distribution because of preliminary data, security classification, or other reasons.

CONTRACTOR REPORTS: Technical information generated in connection with a NASA contract or grant and released under NASA auspices.

TECHNICAL TRANSLATIONS: Information published in a foreign language considered to merit NASA distribution in English.

TECHNICAL REPRINTS: Information derived from NASA activities and initially published in the form of journal articles.

SPECIAL PUBLICATIONS: Information derived from or of value to NASA activities but not necessarily reporting the results of individual NASA-programmed scientific efforts. Publications include conference proceedings, monographs, data compilations, handbooks, sourcebooks, and special bibliographies.

Details on the availability of these publications may be obtained from:

SCIENTIFIC AND TECHNICAL INFORMATION DIVISION
NATIONAL AERONAUTICS AND SPACE ADMINISTRATION
Washington, D.C. 20546